# Quantitative Holocene climatic reconstructions for the lower Yangtze region of China

**Jianyong Li** [1, *] • **John Dodson** [1, 2, *] • **Hong Yan** [1, *] • **Weiming Wang** [3, *] • **James B. Innes** [4, *] • **Yongqiang Zong** [5, 6] • **Xiaojian Zhang** [7] • **Qinghai Xu** [8] • **Jian Ni** [9] • **Fengyan Lu** [1]

[1] State Key Laboratory of Loess and Quaternary Geology, Institute of Earth Environment, Chinese Academy of Sciences, Xi'an 710075, China. [2] School of Biological, Earth and Environmental Sciences, University of New South Wales, Sydney 2033, Australia. [3] Key Laboratory of Economic Stratigraphy and Palaeogeography, Nanjing Institute of Geology and Palaeontology, Chinese Academy of Sciences, Nanjing 210008, China. [4] Geography Department, Durham University, Durham DH1 3LE, UK. [5] Department of Earth Sciences, The University of Hong Kong, Hong Kong Special Administrative Region, China. [6] Guangzhou Institute of Geography, Guangzhou 510070, China. [7] School of Geographic and Oceanographic Sciences, Nanjing University, Nanjing 210093, China. [8] Institute of Nihewan Archaeology, Hebei Normal University, Shijiazhuang 050024, China. [9] College of Chemistry and Life Sciences, Zhejiang Normal University, Jinhua 321004, China.

[*]Correspondence authors: **Jianyong Li** (lijy@ieecas.cn), **John Dodson** (john@ieecas.cn), **Hong Yan** (yanhong@ieecas.cn), **Weiming Wang** (wmwang@nigpas.ac.cn), and **James B. Innes** (j.b.innes@durham.ac.uk).

Address: State Key Laboratory of Loess and Quaternary Geology, Institute of Earth Environment, Chinese Academy of Sciences, Xi'an 710075, China, telephone number: +86-029-62336270; Key Laboratory of Economic Stratigraphy and Palaeogeography, Nanjing Institute of Geology and Palaeontology, Chinese Academy of Sciences, Nanjing 210008, China; Geography Department, Durham University, Durham DH1 3LE, UK.

## Abstract

Quantitative proxy-based and high-resolution palaeoclimatic datasets are scarce for the lower reaches of the Yangtze River (LYR) basin. This region is in a transitional vegetation zone which is climatologically sensitive; and as a birthplace for prehistorical civilization in China, it is important to understand how palaeoclimatic dynamics played a role in affecting cultural development in the region. We present a pollen-based and regionally-averaged Holocene climatic twin-dataset for mean total annual precipitation (PANN) and mean annual temperature (TANN) covering the last 10,000 years for the LYR region. This is based on the technique of weighted averaging-partial least squares regression to establish robust calibration models for obtaining reliable climatic inferences. The pollen-based reconstructions generally show an early Holocene climatic optimum with both abundant monsoonal rainfall and warm thermal conditions, and a declining pattern of both PANN and TANN values in the middle to late Holocene. The main driving forces behind the Holocene climatic changes in the LYR area are likely summer solar insolation associated with tropical or subtropical macro-scale climatic circulations such as the Intertropical Convergence Zone (ITCZ), Western Pacific Subtropical High (WPSH), and El Niño/Southern Oscillation (ENSO). Regional multi-proxy comparisons indicate that the Holocene variations in precipitation and temperature for the LYR region display an in-phase relationship with other related proxy records from southern monsoonal China and the Indian monsoon-influenced regions, but are inconsistent with the Holocene moisture or temperature records from northern monsoonal China and the westerly-dominated region in northwestern China. Overall, our comprehensive palaeoclimatic dataset and models may be significant tools for understanding the Holocene Asian monsoonal evolution and for anticipating its future dynamics in eastern Asia.



**Keywords:** lower Yangtze, China, Holocene, climate, pollen, quantitative reconstructions


## 1 Introduction

The Yangtze River and its catchment occupy one of the largest drainage-basin systems in eastern Asian continent and act as a boundary zone of northern and southern China (e.g. Zhao and Chen 1999; Wu et al. 2012). The lower reaches of the Yangtze River (LYR) are situated in an area that is dominated by the East Asian monsoonal circulation (EAM); and the natural vegetation is warm temperate broadleaf and subtropical evergreen forests as well as transitions of these biomes (e.g. Ren and Beug 2002; Innes et al. 2014). The vegetation and environment in the LYR region would have been sensitive to even small-scale Holocene climatic as well as sea level fluctuations, due largely to its special bioclimatic locality and any marked weakening or strengthening of the EAM regime (e.g. Morrill et al. 2003; Yi et al. 2003; Zong et al. 2011). In particular, the LYR has been identified as one of the birthplaces for prehistorical Chinese civilization such as the ancient Hemudu and Liangzhu Cultures, and for rice cultivation such as the domesticated paddy *Oryza sativa*, as broadly elucidated by detailed palaeoecological and archaeological evidence obtained in earlier studies (e.g. Londo et al. 2006; Zong et al. 2007; Atahan et al. 2008; Fuller et al. 2009; Zhao et al. 2009; Li et al. 2010). As a consequence, the LYR has thus been suggested as an ideal region of interest for exploring the history of Holocene environmental, climatic, and cultural changes in eastern monsoonal China (e.g. Chen et al. 2005, 2009; Innes et al. 2009, 2014; Wang et al. 2011, 2012; Zong et al. 2007, 2011, 2012).

Quantitatively-integrated and high-resolution records of Holocene precipitation and temperature variations are rarely available in the LYR region, and the nature of Holocene climatic evolution in this region remains unclear (e.g. An et al. 2000; Yi et al. 2003; Chen et al. 2005; Zong et al. 2006; Atahan et al. 2008; Innes et al. 2009; Shu et al. 2010; Zong et al. 2011, 2012). Several questions arise, including (i) has the Holocene climate evolved similarly or differently between the LYR and other EAM-affected regions of China such as northern monsoonal China? (ii) What potential driving factors have possibly triggered the Holocene climatic oscillations in the LYR? (iii) Have precipitation and temperature patterns behaved synchronously or asynchronously during the course of Holocene in the LYR? (iv) What was the timing and magnitude of the Holocene climatic optimum in the LYR? Making progress on these issues requires regional-scale, high-resolution, and numerical palaeoclimatic data.

Quantitative palaeoclimatological estimates using biological fossil proxies preserved in sediments provide an important avenue to develop these climatic data for comparison with regionally-averaged

and temporally-detailed Holocene precipitation as well as temperature data in northern China (e.g. Xu et al. 2010; Chen et al. 2015; Li et al. 2015, 2017), the Tibetan Plateau (e.g. Shen et al. 2008; Herzschuh et al. 2009; Wang et al. 2014), and many regions of Europe and North America (e.g. Seppä et al. 2009; Bartlein et al. 2011; Viau et al. 2012; Heiri et al. 2014; Mauri et al. 2015; Ladd et al. 2015), at local, regional, and continental scales. The continuous and conceptual advances in developing and improving large-scale calibration datasets and novel statistical techniques, have greatly promoted the accuracy and robustness of climatic reconstructions, with different means of transforming a variety of fossil biological assemblages into numerical estimates of past rainfall and temperature during the Holocene (e.g. Birks et al. 2010; Salonen et al. 2014; Wang et al. 2014; Li et al. 2015, 2017). Such reconstructed climatic data are particularly valuable for validating climatic transient-model simulations and other independent climatic proxies comprising various geophysical, geochemical, and geoecological records from both terrestrial and marine environments worldwide (e.g. Braconnot et al. 2012; Renssen et al. 2012; Heiri et al. 2014; Li et al. 2015, 2017). In this respect, pollen data are one of the most commonly-used biological proxies for quantitative Holocene terrestrial climatic inferences at a broad scale (e.g. Seppä et al. 2009; Birks et al. 2010; Wang et al. 2014; Li et al. 2017).

In view of the above, we place a key focus on reporting new, high-resolution Holocene precipitation and temperature reconstructions based on three fossil pollen sequences located within the lower Yangtze region of monsoonal China. Our main purpose is to enable a broader understanding and discussion with respect to the Holocene climate-related issues presented above regarding the LYR and monsoonal China. We further assess our pollen-based Holocene climatic reconstructions by relying upon an extensive multi-proxy comparison with a large number of either single or integrated moisture- and temperature-related proxy records from China as well as other regions of the world, such as speleothem oxygen isotope records (e.g. Fleitmann et al. 2003; Wang et al. 2005), loess-palaeosol sequences (e.g. Wang et al. 2014; Li et al. 2014), lake sediment cores (e.g. Shen et al. 2005; Chen et al. 2015), and climate model simulations (e.g. Jin et al. 2013; Chen et al. 2014). Moreover, the most important element of this study is to contribute improved and meaningful insights for evaluating the role of causal forces and atmospheric circulations in driving Holocene climatic, environmental, and cultural changes as well as on forecasting their future possible dynamics in the lower Yangtze region

of China.

## 2 Study area

The lower valley of the Yangtze basin is located in the eastern part of monsoonal China (Fig. 1), where the Asian monsoon dominates the climate and is characterized by warm, wet monsoon in summertime and cold, dry monsoon in wintertime, with four well-pronounced climatic seasons occurring per year. The 700 hPa atmospheric airstream lines in Figure 1 clearly show that the lower Yangtze region is under the typical influence of the East Asian summer monsoon system, whilst northwestern and southwestern China are dominated by the westerlies and Indian summer monsoon circulation, respectively. Mean annual temperature (TANN) varies between 14.5 and 16.2 °C, and mean total annual precipitation (PANN) ranges from 800 to 1400 mm, with its maximum level taking place in July (e.g. Yi et al. 2006; Li et al. 2012). The area of our investigation is naturally covered by a high-density of water-bodies including lakes, peats, bogs, marshes, swamps and wetlands, and it has thus been particularly attractive for palaeoenvironmental studies (e.g. Tao et al. 2006; Innes et al. 2009, 2014; Wang et al. 2011, 2012). The vegetation of the LYR area is a biogeographical ecotone consisting of mixed broad leaved deciduous and evergreen forests with distinct transitional characteristics (e.g. Wu 1983; Huang and Zhang 2000). The main temperate components comprise species of *Betula*, *Ulmus*, *Alnus*, *Populus*, *Quercus*, and *Acer*. The dominant evergreen components include *Castanopsis*, *Cyclobalanopsis*, *Lithocarpus*, and Fagaceae. In addition, a low number of coniferous plant taxa such as *Pinus*, *Picea*, and Cupressaceae occur in the high-elevation mountainous areas (e.g. Zong et al. 2011, 2012). It is therefore likely that in the transitional vegetation belt of the LYR, the Holocene climatic variability would have caused a northward or southward shift of the temperate or subtropical biome because of fluctuations in precipitation as well as temperature controlled primarily by the overall variability of Eastern Asian summer monsoonal (EASM) intensity (e.g. Yi et al. 2006; Zong et al. 2007, 2011).

## 3 Materials and methods

Pollen-based quantitative estimates for both PANN and TANN were prepared from three Holocene pollen datasets at Chaohu (Chen et al. 2009), Gucheng (Yang et al. 1996), and Pingwang (Innes et al.

2014), that lie within the lower reaches of the Yangtze catchment (Fig. 1). These fossil pollen profiles were selected as they have reliable chronological control and fine-scale temporal resolution (see Table 1 for other details). The AMS radiocarbon technique was utilized to create geochronological datasets (Yang et al. 1996; Chen et al. 2009; Innes et al. 2014). Plant macrofossils, shell fragments, pollen residues, charcoal particles, and basal peats have been used for AMS dating (Yang et al. 1996; Chen et al. 2009; Innes et al. 2014). The age–depth models were estimated by a linear interpolation between adjacent samples (Yang et al. 1996; Chen et al. 2009; Innes et al. 2014). The radiocarbon dates were calibrated and transformed to calendar years before present according to the IntCal13 calibration dataset (Reimer et al. 2013). The AMS $^{14}C$ dates are presented here as cal. yr BP throughout the text. The three fossil sites are geographically very close to each other, suggesting that they have probably witnessed similar climatic histories during the Holocene.

Pollen-based numerical calibration models for both PANN and TANN were established using the Chinese surface pollen–climate database which has been shown to be robust and reliable for Holocene climatic inferences that have been described elsewhere in more detail (e.g. Zheng et al. 2008, 2014; Li et al. 2014, 2015, 2017). The technique in terms of weighted averaging-partial least squares (WA-PLS; ter Braak and Juggins 1993) regression and calibration was chosen for constructing the pollen-based reconstruction models for PANN as well as TANN, because it has been successfully employed in a large number of empirical, theoretical and practical studies; and has been shown to perform as well as or better in comparison with other statistical regression approaches that are commonly applied for developing pollen-based calibration models for regional, continental and global scales (e.g. Birks 1998; Seppä et al. 2009; Birks et al. 2010; Salonen et al. 2012; Li et al. 2015, 2017). The performance of all WA-PLS models was assessed with the method of leave-one-out cross-validation (Birks 1998). The calculated model statistics for PANN and TANN embrace coefficient of determination ($R^2$) between measured and predicted data, root-mean-square-error of prediction (RMSEP), and maximum bias. The two-component WA-PLS models (Fig. 2) were selected with respect to high $R^2$, low RMSEP and maximum bias, as well as the smallest number of useful components (Birks 1998). All terrestrial pollen taxa were taken into account and their percentage values were square-root transformed to reduce noises and stabilize variances in the pollen data (Prentice 1980). The constructions or evaluations of all WA-

PLS models associated with the numerical PANN or TANN estimates were carried out using the C2 software (Juggins 2007). In addition, it has been demonstrated elsewhere that PANN and TANN are not always strongly correlated and that either PANN or TANN is statistically significant as well as ecologically meaningful in influencing broad-scale pollen distribution, indicating that they can be employed simultaneously for the pollen-based palaeoclimatic reconstructions applied here (e.g. Li et al. 2014, 2015).

To obtain the underlying characteristics and summarize the potential regional signals, a total of six quantitative climatic reconstructions based on the three fossil pollen datasets were integrated to produce two general high-resolution Holocene climatic sequences (PANN and TANN) for the lower Yangtze region of China. Such a composite methodology has been successfully used for quantitative pollen-derived and regional-scale Holocene climatic reconstructions in Europe (e.g. Seppä et al. 2009; Salonen et al. 2014; Mauri et al. 2015), North America (e.g. Viau et al. 2006, 2012; Ladd et al. 2015), and northern China (e.g. Li et al. 2015, 2017). It can be described briefly as follows. Each PANN or TANN estimate was calculated as deviations from their mean values across the Holocene. All estimated values of individual reconstructions for PANN or TANN were then combined so as to prepare two Holocene climatic records with an average time-resolution of circa 36 years for both PANN and TANN. Power spectra for potential periodicities in the pollen-stacked precipitation and temperature records were performed using the Redfit software (Schulz and Mudelsee 2002). This software is able to deal with unevenly distributed time-series data, and can test statistical significance of the spectral peaks against the red-noise background with a null-hypothesis, which can be evaluated by utilizing the first-order autoregressive signals, where characteristic time-scales as well as sampled time-spans match those of the real data, without the necessity for any interpolation (Schulz and Mudelsee 2002).

# 4 Results and discussion

## 4.1 Climatic reconstructions with low- and high-frequency trends

The pollen-inferred site-specific Holocene climatic reconstructions are presented in Figure 3. The regionally-averaged estimates are shown in Figure 4. Thus we provide the first ~36-year resolution

pairwise-dataset for both PANN and TANN records covering the last 10,000 years. These portray both general patterns as well as detailed features of the Holocene rainfall and temperature variations for the lower reaches of the Yangtze catchment. Power spectrum analyses conducted for the composite reconstructions reveal significant periodicities of 4000, 1190, and 116 years for PANN, and of 2500, 1190, and 116 years for TANN (Fig. 5). Some of these periodicities can also be found in other Holocene Asian monsoonal records and various solar parameters (e.g. Li et al. 1996; Laskar et al. 2004; Dykoski et al. 2005; Wang et al. 2008; Wanner et al. 2008, 2011; Zhao and Feng 2014), suggesting a possible mechanistic connection among these climatic systems.

Overall high-frequency PANN and TANN fluctuations concurrently show a maximum level between 10,000 and 7000 cal. yr BP, and a generally declining pattern with strong oscillations from 7000 cal. yr BP to the present-day (Fig. 4). The early to middle Holocene had high values of PANN and TANN, suggesting a warm, wet climate and a strong East Asian summer monsoon, as also demonstrated by rapidly increased sea level and possible small paddy rice cultivation in the LYR coastal plain (e.g. Innes et al. 2009; Shu et al. 2010; Zong et al. 2011; Wang et al. 2012). Subtropical forests were regarded as the dominant regional biome during this time phase, with *Castanopsis* and *Cyclobalanopsis* identified as the major tree taxa, which is evident in many published fossil pollen records from different parts of the LYR region (e.g. Chen et al. 2005; Yi et al. 2006; Innes et al. 2009; Wu et al. 2010; Li et al. 2012). However, since approximately 7000~5000 cal. yr BP, the cool temperate forest elements such as *Quercus*, *Betula* and *Alnus* started to occur and expanded while subtropical elements decreased, eventually leading to a mixed temperate–evergreen vegetation type which prevailed until modern times. The relative sea level was stable with only small fluctuations observed for this time period (e.g. Huang and Zhang 2000; Shu et al. 2007; Yi et al. 2006; Innes et al. 2014). This is closely in line with our climatic reconstructions displaying a falling trend for PANN and TANN values during this period, implying a cooling and drying climate associated with a gradually weakening EASM intensity from the middle to late Holocene in the LYR area (Fig. 4). In addition, it is noteworthy that in eastern monsoonal China, human activity played an important role in influencing vegetation cover during the late Holocene especially the last 2000 years (e.g. Zhao et al. 2009), which implies that pollen-based climatic inferences should thus be treated with caution (e.g. Li et al. 2014).

Several low-frequency cooling and drying episodes can be clearly detected from our pollen-estimated PANN and TANN records. These cold and dry climatic events at about 5300, 4200, 2800 cal. yr BP and during the Little Ice Age interval in the LYR region (Fig. 4) appear to be correlated well with those widely reported from other areas in China (e.g. Wang et al. 2005; Shao et al. 2006; Xu et al. 2010; Innes et al. 2014), the North Atlantic region (e.g. Bond et al. 2001; Seppä et al. 2009), and the Northern Hemisphere (e.g. Clemens 2005; Viau et al. 2006; Wanner et al. 2008, 2011). Such short-lived climatic events with high amplitude have been suggested to play a significant role in driving the demise and termination of Neolithic civilization such as the Liangzhu Culture in the Yangtze lowland area, because prehistorical farming fields and human settlements were usually situated close to water bodies such as lake shores and river channels, leading to these agricultural lands and cultural systems becoming vulnerable to abrupt changes in water supplies and thermal conditions during the Holocene, for example during the Neoglacial epoch (e.g. Zhang et al. 2005; Yao et al. 2008; Huang et al. 2010; Wu et al. 2010; Innes et al. 2014).

### 4.2 Comparison with other subtropical or tropical Holocene records and possible mechanisms

A decadal- to centennial-scale comparison of our pollen-based PANN and TANN estimates for the LYR with other related Holocene climatic proxy records from subtropical China, the Indian summer monsoon (ISM)-influenced region and other tropical or subtropical regions of the world, indicates a macro-scale in-phase pattern of general variability, exhibiting a consistent early Holocene climatic optimum in precipitation or temperature but a relatively dryer or cooler middle to late Holocene (Fig. 6). However, it is notable that this general pattern is different to that indicated by two Holocene hydrological records from the middle reaches of the Yangtze River, that is, the mass accumulation rates of hopanoids from Dajiuhu peat bog as a proxy for water level, and the ratio of anhysteretic remanent magnetization (ARM) to saturation isothermal remanent magnetization (SIRM) from a stalagmite in Heshang Cave as a magnetic proxy, both suggesting a dry middle Holocene but a wetter early or late Holocene (Xie et al. 2013). These two records are also inconsistent with other proxy-based climatic records from the same region, for example, the pollen-based TANN record from Dajiuhu peat (Zhu et al. 2008) and the stalagmite $\delta^{18}O$ record from Heshang Cave (Hu et al. 2008), which are in good agreement with our Holocene PANN and TANN records for the LYR. This discrepancy may result

246 from the differences in the various reconstruction techniques, distinct temporal resolutions, reliability
247 of sedimentary chronologies, climatic significance of diverse proxy indicators, or spatial
248 representativeness of sampled sites (e.g. Liu et al. 2015; Rao et al. 2016; Chen et al. 2016a). In addition,
249 the aforementioned Holocene climatic records with consistent patterns that cover a broad geographical
250 region include the following proxy datasets: the mean summer solar insolation (Laskar et al. 2004);
251 stalagmite $\delta^{18}O$ records from Dongge (Dykoski et al. 2005), Sanbao (Wang et al. 2008) and Qunf
252 (Fleitmann et al. 2003) Caves; a model-simulated PANN record for southwestern China (Chen et al.
253 2014); a pollen-inferred PANN estimate for Xingyun Lake in the ISM-influenced Yunan Province
254 (Chen et al. 2014); a TANN reconstruction from Dajiuhu wetland in the EASM-dominated Hubei
255 Province (Zhu et al. 2008); pollen-estimated moisture index (Zhao et al. 2009) as well as tree cover
256 reconstruction (Tian et al. 2016) for southern China; a humification record from Hongyuan wetland on
257 the southeastern Tibetan Plateau (Yu et al. 2006); a synthesized moisture index based on various proxy
258 data for the southern Tibetan Plateau (Ran and Feng 2013); total organic carbon (Yancheva et al. 2007)
259 and tree pollen records (Wang et al. 2007) from Huguangyan Maar Lake in southern China; an ISM
260 rainfall index based on 92 monsoonal moisture records in eastern Asia (Wang et al. 2010); the
261 Intertropical Convergence Zone (ITCZ) index inferred from Ti contents in Cariaco Basin, Venezuela
262 (Haug et al. 2001); a *Globigerina bulloides* record from a marine sediment core in Arabian Sea (Gupta
263 et al. 2005); composite sea surface temperature (SST) records for Western Pacific Warm Pool (WPWP;
264 Scott et al. 2004; Koutavas and Joanides 2012); and an El Niño/Southern Oscillation (ENSO) record
265 from Laguna Pallcacocha, Ecuador (Moy et al. 2002). Of these records, it is worth noting that the
266 Holocene stalagmite $\delta^{18}O$ data have been lately argued to probably represent a signal of the isotopic
267 composition of precipitation from the ISM-influenced region rather than the EASM-dominated
268 territory (e.g. Chen et al. 2014; Yang et al. 2014; Wang et al. 2014; Liu et al. 2015; Chen et al. 2016a).
269 The above multiple lines of evidence suggest a strong causal linkage between tropical and
270 subtropical climatic systems from the perspective of hemispheric or global scale teleconnections (Fig.
271 6). It has been often proposed in earlier studies that the orbitally-controlled variability of summer solar
272 insolation would have essentially modulated and triggered the tropical and subtropical summer
273 monsoonal evolution during the post-glacial Holocene epoch (e.g. An et al. 2000; Gupta et al. 2005;

Fleitmann et al. 2003; Wang et al. 2008; Zhao et al. 2009; Koutavas and Tsukamoto 2014). During the early Holocene, the high output of summer insolation may have caused the northward migration of both mean ITCZ and Western Pacific Subtropical High (WPSH) positions as indicated clearly by the high SST values in the WPWP and the Arabian Sea. This therefore resulted in a great amount of evaporated water vapor being transported from the tropical and subtropical oceanic areas to southern and eastern Asia, leading to the northward expansion and penetration of the overall summer monsoonal strength as well as its extensive rain band, and thus abundant rainfall as well as high temperature in the low-latitude regions of monsoonal Asia (e.g. Scott et al. 2004; Zhao et al. 2007; Zhou et al. 2009; Sun and Feng 2013). In contrast, during the middle to late Holocene, a reduced summer insolation would have brought about the southward retreat of both ITCZ and WPSH zones along with the decreased pattern of tropical SST values, which led to a lower moisture transportation from the ocean to continental lands, thereby causing the southward shift and weakening of the summer monsoonal intensity and its rain belt, and reduced rainfall as well as lower heat content in the southern part of monsoonal Asia and China (e.g. Dykoski et al. 2005; Wang et al. 2008; Sun and Feng 2013). In addition, an overall stepwise intensification of ENSO activity from the early to late Holocene (Fig. 6) has been suggested to bring warm water masses with higher SST to the eastern Tropical Pacific Ocean, resulting in lower SST in the western Tropical Pacific Ocean, thus progressively reducing the transport of water vapor to monsoonal China during the entire Holocene (e.g. Wang et al. 2000; Higginson et al. 2004; Sun and Feng 2013).

### 4.3 Comparison with Holocene climatic records from northern monsoonal and the westerlies' region of China

A detailed comparison of our inferred precipitation and temperature reconstructions for the LYR with other high-resolution Holocene moisture and temperature records in the monsoonal regions of northern China and in the westerly-dominated areas of northwestern China, reveal an out-of-phase pattern of overall climatic shifts and a major offset in relation to timings of the Holocene climatic optimum interval (Fig. 7). These early published records consist of the following datasets: pollen-reconstructed annual rainfall series from Gonghai Lake (Chen et al. 2015) on the Chinese Loess Plateau (CLP) and Daihai Lake (Xu et al. 2010) in central Inner Mongolia; a multi-proxy based temperature

reconstruction for northern China (Hou and Fang 2011); an EASM index based on various proxies in the northern part of monsoonal China (Wang et al. 2010); tree pollen percentages from Qinghai Lake (Shen et al. 2005) and Bayanchagan Lake (Jiang et al. 2006) in northern monsoonal China; a pollen-based moisture record for the northern EASM marginal region (Wang and Feng 2013); frequencies of palaeosol occurrences in the CLP (Wang et al. 2014) and northern China (Li et al. 2014); frequency in the formation of loess or aeolian sands in northern China (Li et al. 2014); a magnetic susceptibility record from the Yulin loess–palaeosol section on the northern CLP (Lu et al. 2013); and a moisture index synthesized from different proxy records for the westerly-influenced regions of Arid Central Asia (ACA) including northwestern China (Chen et al. 2008).

The multiple Holocene climatic records, spanning a large geographical area in both northern and northwestern China, point to an overwhelming signal with respect to a middle Holocene climatic optimum that is characterized by the highest precipitation amounts or the warmest temperature conditions (Fig. 7). Recently, Chen et al. (2016b) indicated that in the Xinjiang region as a core area of ACA, magnetic susceptibility records from four loess–palaeosol profiles have exhibited an increasing moisture pattern from the early to late Holocene. However, these trends are out-of-phase with a typical signal of an early Holocene climatic optimum demonstrated by our pollen-stacked PANN or TANN reconstructions for the LYR region as well as other Holocene monsoonal records from the subtropical and tropical domains of China or the ISM-dominated regions presented in this study (Fig. 6). Such an inconsistency may have arisen from unreliable dating controls, various proxy interpretations and resolutions, or different methodological issues and assumptions (e.g. Zhao et al. 2009; Cai et al. 2010; Sun and Feng 2013; Liu et al. 2015). In addition, the climatological viewpoints with regard to this notable timing mismatch remain under debate, which can be tentatively attributed to the significant cooling effect at a hemispherical-scale caused by the deglaciation of broad-scale remnant ice sheets in the high-latitude territories of the Northern Hemisphere during the early Holocene (Fig. 7) (e.g. Chen et al. 2008; Renssen et al. 2012; Li et al. 2015; Liu et al. 2015; Mjell et al. 2015). The rapid melting of these remnant ice sheets such as the Laurentide Ice Sheet (Jennings et al. 2015) in North America and the Agassiz Ice Cap (Fisher et al. 2012) in Greenland, would have likely yielded a large body of freshwater discharge into the northern Atlantic Ocean (Fig. 7). This may

have resulted in a suppressed Atlantic meridional overturning circulation (AMOC) as well as North Atlantic Deep Water circulation (NADW), and at the same time increased Ice-Rafted Debris (IRD) in ocean sediments, massive glacial advances, strong meridional temperature gradient and westerly airstreams, and intensified Siberian High and winter monsoon strength, which may in turn have played an important role in blocking the northward movements of the summer monsoon as well as its rainfall front to the northern part of monsoonal China during the early Holocene (Fig. 7) (e.g. Zhao et al. 2009; Chen et al. 2015; Li et al. 2015; Liu et al. 2015).

## Conclusions

Here we present a pollen-based Holocene climatic dataset with a ~36-year resolution for both PANN and TANN records over the last 10,000 years for the lower reaches of the Yangtze basin in eastern monsoonal China. Our reconstructions show that precipitation and temperature have a concurrent trend of variability on a centennial- to multidecadal timescale, implying a notable climatic pattern of moist-warm or dry-cool intervals during the Holocene. Multi-proxy comparisons indicate that regional-scale Holocene rainfall and thermal variations in the lower Yangtze area are in good agreement with other Holocene climatic records from southern monsoonal China or the ISM-dominated regions, suggesting an early Holocene climatic optimum that was characterized by high precipitation and warm conditions, and a drying or cooling climate for the middle to late Holocene. The orbitally-triggered changes of summer solar insolation and tropical or subtropical climatic circulations such as ITCZ, WPSH, and ENSO may be recognized as the important driving factors for the Holocene summer monsoon variability in the lower Yangtze region of China. Further regional inter-comparisons reveal that the LYR Holocene climatic development has been different to the Holocene moisture or thermal records from the EASM-influenced northern China and the westerly-affected northwestern China where the Holocene climatic optimum mostly took place during the middle Holocene. Overall, our pollen-based high-resolution climatic dataset may be useful for validating climate model simulations, understanding the nature of monsoon climate, and predicting future climatic scenarios in monsoonal Asia and its surrounding areas. Clearly, more case studies would enhance understanding the nature of Holocene climatic changes in different bioclimatic regions of monsoonal China.

## Acknowledgments

This work was financially funded by projects from the State Key Laboratory of Loess and Quaternary Geology in the Institute of Earth Environment of the Chinese Academy of Sciences (Y652001589 and Y651031589), the West Light Foundation of The Chinese Academy of Sciences (XAB2016B01), the National Science Foundation of China (NSFC 41522305 and 41403018), the Major State Basic Research Development Program (973 Program) of China (2013CB955900), and other projects from the Chinese Academy of Sciences (QYZDB-SSW-DQC001, 132B61KYSB20160003, and 55ZZBS1304101).

## References

An ZS (2000) The history and variability of the East Asian paleomonsoon climate. Quat Sci Rev 19:171–187

Atahan P et al. (2008) Holocene-aged sedimentary records of environmental changes and early agriculture in the lower Yangtze, China. Quat Sci Rev 27:556–570

Bartlein PJ et al (2011) Pollen-based continental climate reconstructions at 6 and 21 ka: a global synthesis. Clim Dyn 37:775–802

Birks HJB (1998) Numerical tools in palaeolimnology: progress, potentialities, and problems. J Paleolimnol 20:307–332

Birks HJB, Heiri O, Seppä H, Bjune AE (2010) Strengths and weaknesses of quantitative climate reconstructions based on late-Quaternary biological proxies. Open Ecol J 3:68–110

Bond G, Kromer B, Beer J, Muscheler R, Evans MN, Showers W, Hoffmann S, Lotti-Bond R, Hajdas I, Bonani G (2001) Persistent solar influence on North Atlantic climate during the Holocene. Science 278:1257–1266

Braconnot P, Harrison S, Kageyama M, Bartlein J, Masson V, Abe-Ouchi A, Otto-Bliesner B, Zhao Y (2012) Evaluation of climate models using palaeoclimatic data. Nat Clim Change 2:417–424

Cai YJ, Tan LC, Cheng H, An ZS, Edwards RL, Kelly MJ, Kong XG, Wang XF (2010) The variation of summer monsoon precipitation in central China since the last deglaciation. Earth Planet Sci Lett 291:21–31

384 Chen FH et al (2008) Holocene moisture evolution in arid central Asia and its out-of-phase relationship
385 with Asian monsoon history. Quat Sci Rev 27:351–364
386 Chen FH et al (2015) East Asian summer monsoon precipitation variability since the last deglaciation.
387 Sci Rep 5:11186
388 Chen FH, Chen XM, Chen JH, Zhou AF, Wu D, Tang LY, Zhang XJ, Huang XZ, Yu JQ (2014)
389 Holocene vegetation history, precipitation change and Indian summer monsoon evolution
390 documented by Xingyun Lake, Southwest China. J Quat Sci 29:661–674
391 Chen FH, Jia J, Chen JH, Li GQ, Zhang XJ, Xie HC, Xia DS, Huang W, An CB (2016b) A persistent
392 Holocene wetting trend in arid central Asia, with wettest conditions in the late Holocene, revealed
393 by multi-proxy analyses of loess-paleosol sequences in Xinjiang, China. Quat Sci Rev 146:134–
394 146
395 Chen FH, Wu D, Chen JH, Zhou AF, Yu JQ, Shen J, Wang SM, Huang XZ (2016a) Holocene moisture
396 and East Asian summer monsoon evolution in the northeastern Tibetan Plateau recorded by Lake
397 Qinghai and its environs: A review of conflicting proxies. Quat Sci Rev 154:111–129
398 Chen W, Wang W, Dai X (2009) Holocene vegetation history with implications of human impact in
399 the Lake Chaohu area, Anhui Province, East China. Veget Hist Archaeobot 18:137–146
400 Chen Z, Wang Z, Schneiderman J, Tao J, Cai Y (2005) Holocene climate fluctuations in the Yangtze
401 delta of eastern China and the Neolithic response. Holocene 15:915–924
402 Clemens SC (2005) Millennial-band climate spectrum resolved and linked to centennial-scale solar
403 cycles. Quat Sci Rev 24:521–531
404 Dyke AS (2004) An outline of North American deglaciation with emphasis on central and northern
405 Canada. Dev Quat Sci 2:373–424
406 Dykoski CA, Edwards RL, Cheng H, Yuan DX, Cai YJ, Zhang ML, Lin YS, Qing JM, An ZS,
407 Revenaugh J (2005) A high-resolution, absolute-dated Holocene and deglacial Asian monsoon
408 record from Dongge Cave, China. Earth Planet Sci Lett 233:71–86
409 Fisher D, Zheng J, Burgess D, Zdanowicz C, Kinnard C, Sharp M, Bourgeois J (2012) Recent melt
410 rates of Canadian arctic ice caps are the highest in four millennia. Glob Planet Change 84–85:3–
411 7

412 Fleitmann D, Burns SJ, Mudelsee M, Neff U, Kramers J, Mangini A, Matter A (2003) Holocene forcing
413 of the Indian monsoon recorded in a stalagmite from southern Oman. Science 300:1737–1739
414 Fuller DQ, Qin L, Zheng Y, Zhao Z, Chen X, Hosoya LA, Sun GP (2009) The domestication process
415 and domestication rate in rice: spikelet bases from the lower Yangtze. Science 323:1607–1610
416 Gupta AK, Das M, Anderson DM (2005) Solar influence on the Indian summer monsoon during the
417 Holocene. Geophys Res Lett 32:L17703
418 Haug GH, Hughen KA, Sigman DM, Peterson LC, Röhl U (2001) Southward migration of the
419 Intertropical Convergence Zone through the Holocene. Science 293:1304–1308
420 Heiri O et al (2014) Validation of climate model-inferred regional temperature change for late-glacial
421 Europe. Nat Commun 5:4914
422 Herzschuh U, Kramer A, Mischke S, Zhang CJ (2009) Quantitative climate and vegetation trends since
423 the late glacial on the northeastern Tibetan Plateau deduced from Koucha Lake pollen spectra.
424 Quat Res 71:162–171
425 Higginson MJ, Altabet MA, Lauren W, Herbert TD, Murray DW (2004) A solar (irradiance) trigger
426 for millennial-scale abrupt changes in the southwest monsoon? Paleoceanography 19:77–100
427 Hou GL, Fang X (2011) Characteristics analysis and synthetical reconstruction of regional temperature
428 series of the Holocene in China. J Palaeogeogr 14:243–252 (in Chinese)
429 Hu CY, Henderson GM, Huang JH, Xie SC, Sun Y, Johnson KR (2008) Quantification of Holocene
430 Asian monsoon rainfall from spatially separated cave records. Earth Planet Sci Lett 266:221–232
431 Huang CC, Pang J, Zha XC, Zhou Y, Su H, Li Y (2010) Extraordinary floods of 4100–4000 a BP
432 recorded at the Late Neolithic ruins in the Jinghe River Gorges, middle reach of the Yellow River,
433 China. Palaeogeogr Palaeoclimatol Palaeoecol 289:1–9
434 Huang F, Zhang M (2000) Pollen and phytolith evidence for rice cultivation during the Neolithic at
435 Longqiuzhuang, eastern Jianghuai, China. Veget Hist Archaeobot 9:161–168
436 Innes JB, Zong Y, Chen Z, Chen C, Wang Z, Wang H (2009) Environmental history, palaeoecology
437 and human activity at the early Neolithic forager/cultivator site at Kuahuqiao, Hangzhou, eastern
438 China. Quat Sci Rev 28:2277–2294
439 Innes JB, Zong Y, Wang Z, Chen Z (2014) Climatic and palaeoecological changes during the mid- to

late Holocene transition in eastern china: high-resolution pollen and non-pollen palynomorph analysis at Pingwang, Yangtze coastal lowlands. Quat Sci Rev 99:164–175

Jennings A, Andrews J, Pearce C, Wilson L, Olfasdotttir S (2015) Detrital carbonate peaks on the Labrador shelf, a 13–7 ka template for freshwater forcing from the Hudson Strait outlet of the Laurentide Ice Sheet into the subpolar gyre. Quat Sci Rev 107:62–80

Jiang W, Guo Z, Sun X, Wu H, Chu G, Yuan B, Hatté C, Guiot J (2006) Reconstruction of climate and vegetation changes of Lake Bayanchagan (Inner Mongolia): Holocene variability of the East Asian monsoon. Quat Res 65:411–420

Jin LY, Schneider B, Park W, Latif M, Khon V, Zhang XJ (2013) The spatial–temporal patterns of Asian summer monsoon precipitation in response to Holocene insolation change: a model-data synthesis. Quat Sci Rev 85:47–62

Juggins S (2007) C2 Version 1.5 User guide. Software for ecological and palaeoecological data analysis and visualisation. Newcastle University, Newcastle upon Tyne

Kalnay E, Kanamitsu M, Kistler R, Collins W, Deaven D, Gandin L, Iredell M, Saha S, White G, Woollen J, Zhu Y, Leetmaa A, Reynolds R (1996) The NCEP/NCAR 40-year reanalysis project. Bull Am Meteorol Soc 77:437–472

Komatsu T, Tsukamoto S (2014) Late Glacial lake-level changes in the Lake Karakul basin (a closed glacierized-basin), eastern Pamirs, Tajikistan. Quat Res 83:137–149

Koutavas A, Joanides S (2012) El Niño-Southern Oscillation extrema in the Holocene and Last Glacial Maximum. Paleoceanography 27:PA4208

Ladd M, Way RG, Viau AE (2015) The impact of using different modern climate data sets in pollen-based paleoclimate reconstructions of north America. Quat Sci Rev 112:78–85

Laskar J, Robutel P, Joutel F, Gastineau M, Correia ACM, Levrard B, (2004) A long term numerical solution for the insolation quantities of the Earth. Astron Astrophys 428:261–285

Li C, Zheng Y, Yu S, Li Y, Shen H (2012) Understanding the ecological background of rice agriculture on the Ningshao plain during the Neolithic age: pollen evidence from a buried paddy field at the Tianluoshan cultural site. Quat Sci Rev 35:131–138

Li JY et al (2015) East Asian summer monsoon precipitation variations in China over the last 9500

468 years: a comparison of pollen-based reconstructions and model simulations. Holocene 26:592–
469 602
470 Li JY et al (2017) Quantifying climatic variability in monsoonal northern China over the last 2200
471 years and its role in driving Chinese dynastic changes. Quat Sci Rev 159:35–46
472 Li JY, Zhao Y, Xu QH, Zheng Z, Lu HY, Luo YL, Li YC, Li CH, Seppä H (2014) Human influence as
473 a potential source of bias in pollen-based climate reconstructions. Quat Sci Rev 99:112–121
474 Li KJ, Su TW, Liang HF (1996) Sunspot unit areas: a new parameter describing the long-term solar
475 activity. Chin Sci Bull 49:2511–2516
476 Li Q, Wu H, Yu Y, Sun A, Markovic SB, Guo Z (2014) Reconstructed moisture evolution of the deserts
477 in northern China since the Last Glacial Maximum and its implications for the East Asian Summer
478 Monsoon. Glob Planet Change 121:101–112
479 Li Y, Wu J, Hou S, Shi C, Mo D, Liu B, Zhou L (2010) Palaeoecological records of environmental
480 change and cultural development from the Liangzhu and Qujialing archaeological sites in the
481 middle and lower reaches of the Yangtze River. Quat Int 227: 29–37
482 Liu JB, Chen JH, Zhang XJ, Li Y, Rao ZG, Chen FH (2015) Holocene East Asian summer monsoon
483 records in northern China and their inconsistency with Chinese stalagmite $\delta^{18}O$ records. Earth Sci
484 Rev 148:194–208
485 Londo JP, Chiang YC, Hung KH, Chiang TH, Schaal BA (2006) Phylogeography of Asian wild rice,
486 *Oryza rufipogon*, reveals multiple independent domestications of cultivated rice, *Oryza sativa*.
487 Proc Natl Acad Sci USA 103:9578–9583
488 Lu HY et al (2013) Variation of East Asian monsoon precipitation during the past 21 k.y. and potential
489 $CO_2$ forcing. Geology 41:1023–1026
490 Mauri A, Davis BAS, Collins PM, Kaplan JO (2015) The climate of Europe during the Holocene: a
491 gridded pollen-based reconstruction and its multi-proxy evaluation. Quat Sci Rev 112:109–127
492 Mjell TL, Ninnemann US, Eldevik T, Kleiven HF (2015) Holocene multidecadal- to millennial-scale
493 variations in Iceland-Scotland overflow and their relationship to climate. Paleoceanography
494 30:558–569
495 Morrill C, Overpeck JT, Cole JE (2003) A synthesis of abrupt changes in the Asian summer monsoon

since the last deglaciation. Holocene 13:465–476

Moy CM, Seltzer GO, Rodbell DT, Anderson DM (2002) Variability of El Niño/Southern Oscillation activity at millennial timescales during the Holocene epoch. Nature 420:162–165

Prentice IC (1980) Multidimensional scaling as a research tool in Quaternary palynology: a review of theory and methods. Rev Palaeobot Palynol 31:71–104

Ran M, Feng Z (2013) Holocene moisture variations across china and driving mechanisms: a synthesis of climatic records. Quat Int 313:179–193

Rao ZG, Li YX, Zhang JW, Jia GD, Chen FH (2016) Investigating the long-term palaeoclimatic controls on the δD and $\delta^{18}O$ of precipitation during the Holocene in the Indian and East Asian monsoonal regions. Earth Sci Rev 159:292–305

Reimer PJ et al (2013) IntCal13 and Marine13 radiocarbon Age calibration curves 0–50,000 years cal BP. Radiocarbon 55:1869–1887

Ren G, Beug HJ (2002) Mapping Holocene pollen data and vegetation of China. Quat Sci Rev 21:1395–1422

Renssen H, Seppä H, Crosta , Goosse H, Roche DM (2012) Global characterization of the Holocene Thermal Maximum. Quat Sci Rev 48:7–19

Salonen JS, Ilvonen L, Seppä H, Holmström L, Telford RJ, Gaidamavicius A, Stancikaite M, Subetto D (2012) Comparing different calibration methods (WA/WA-PLS regression and Bayesian modelling) and different-sized calibration sets in pollen-based quantitative climate reconstruction. Holocene 22:413–424

Salonen JS, Luoto M, Alenius T, Heikkilä M, Seppä H, Telford RJ, Birks HJB (2014) Reconstructing palaeoclimatic variables from fossil pollen using boosted regression trees: comparison and synthesis with other quantitative reconstruction methods. Quat Sci Rev 88:69–81

Schulz M, Mudelsee M (2002) REDFIT: estimating red-noise spectra directly from unevenly spaced paleoclimatic time series. Comput Geosci 28:421–426

Seppä H, Bjune AE, Telford RJ, Birks HJB, Veski S (2009) Last nine-thousand years of temperature variability in Northern Europe. Clim Past 5:523–535

Shao X, Wang Y, Cheng H, Kong X, Wu J, Edwards RL (2006) Long-term trend and abrupt events of

524 the Holocene Asian monsoon inferred from a stalagmite d$^{18}$O record from Shennongjia in central
525 China. Chin Sci Bull 51:1–8
526 Shen CM, Liu KB, Morrill C, Overpeck JT, Peng JL, Tang LY (2008) Ecotone shift and major droughts
527 during the mid-late Holocene in the central Tibetan Plateau. Ecology 89:1079–1088
528 Shen J, Liu XQ, Wang SM, Ryo M (2005) Palaeoclimatic changes in the Qinghai Lake area during the
529 last 18,000 years. Quat Int 136:131–140
530 Shu JW, Wang WM, Chen W (2007) Holocene vegetation and environment changes in the NW Taihu
531 plain, Jiangsu Province, East China. Acta Micropalaeontol Sin 24:210–221 (in Chinese)
532 Shu JW, Wang WM, Jiang LP, Takahara H (2010) Early Neolithic vegetation history, fire regime and
533 human activity at Kuahuqiao, Lower Yangtze River, East China: new and improved insight. Quat
534 Int 227:10–21
535 Stott L, Cannariato K, Thunell R, Haug GH, Koutavas A, Lund S (2004) Decline of surface
536 temperature and salinity in the western tropical Pacific Ocean in the Holocene epoch. Nature
537 431:56–59
538 Sun AZ, Feng ZD (2013) Holocene climatic reconstructions from the fossil pollen record at Qigai
539 Nuur in the southern Mongolian Plateau. Holocene 23:1391–1402
540 Tao J, Chen MT, Xu S (2006) A Holocene environmental record from the southern Yangtze River delta,
541 eastern China. Palaeogeogr Palaeoclimatol Palaeoecol 230:204–229
542 ter Braak CJF, Juggins S (1993) Weighted averaging partial least squares regression (WA-PLS): an
543 improved method for reconstructing environmental variables from species assemblages.
544 Hydrobiologia 269:485–502
545 Tian F, Cao X, Dallmeyer A, Ni J, Zhao Y, Wang Y, Herzschuh U (2016) Quantitative woody cover
546 reconstructions from eastern continental Asia of the last 22 kyr reveal strong regional peculiarities.
547 Quat Sci Rev 137:33–44
548 Viau AE, Gajewski K, Sawada MC, Fines P (2006) Millenial-scale temperature variability in North
549 America during the Holocene. J Geophys Res 111:D09102
550 Viau AE, Ladd M, Gajewski K (2012) The climate of north America during the past 2000 years
551 reconstructed from pollen data. Glob Planet Change 84–85:75–83

552 Wang B, Wu R, Fu X (2000) Pacific–East Asia teleconnection: how does ENSO affect East Asian
553 climate? J Clim 13:1517–1536
554 Wang H, Chen J, Zhang X, Chen F (2014) Palaeosol development in the Chinese Loess Plateau as an
555 indicator of the strength of the East Asian summer monsoon: evidence for a mid-Holocene
556 maximum. Quat Int 334:155–164
557 Wang S, Lü H, Liu J, Negendank JW (2007) The early Holocene optimum inferred from a high-
558 resolution pollen record of Huguangyan Maar Lake in southern China. Chin Sci Bull 52:2829–
559 2836
560 Wang W, Feng Z (2013) Holocene moisture evolution across the Mongolian Plateau and its
561 surrounding areas: a synthesis of climatic records. Earth Sci Rev 122:38–57
562 Wang Y et al (2014) Quantitative reconstruction of precipitation changes on the NE Tibetan Plateau
563 since the Last Glacial Maximum e extending the concept of pollen source area to pollen-based
564 climate reconstructions from large lakes. Clim Past 10:21–39
565 Wang Y, Cheng H, Edwards RL, He Y, Kong X, An Z, Wu J, Kelly MJ, Dykoski CA, Li X (2005) The
566 Holocene Asian monsoon: links to solar changes and North Atlantic climate. Science 308:854–
567 857
568 Wang YB, Liu XQ, Herzschuh U (2010) Asynchronous evolution of the Indian and East Asian Summer
569 Monsoon indicated by Holocene moisture patterns in monsoonal central Asia. Earth Sci Rev
570 103:135–153
571 Wang YJ et al (2008) Millennial- and orbital-scale changes in the East Asian monsoon over the past
572 224,000 years. Nature 451:1090–1093
573 Wang Z, Li M, Zhang R, Zhuang C, Liu Y, Saito Y, Xie J, Zhao B (2011) Impacts of human activity
574 on the late-Holocene development of the subaqueous Yangtze Delta, China, as shown by magnetic
575 properties and sediment accumulation rates. Holocene 21:393–407
576 Wang Z, Zhuang C, Saito Y, Chen J, Zhan Q, Wang X (2012) Early mid-Holocene sea-level change
577 and coastal environmental response on the southern Yangtze delta plain, China: implications for
578 the rise of Neolithic culture. Quat Sci Rev 35:51–62
579 Wanner H et al (2008) Mid- to Late Holocene climate change: an overview. Quat Sci Rev 27:1791–

1828

Wanner H, Solomina O, Grosjean M, Ritz SP, Jetel M (2011) Structure and origin of Holocene cold events. Quat Sci Rev 30:3109–3123

Wu L, Li F, Zhu C, Li B (2012) Holocene environmental change and archaeology, Yangtze River Valley, China: review and prospects. Geosci Front 3:875–892

Wu L, Wang XY, Zhou KS, Mo D, Zhu C, Gao C, Zhang G, Li L, Han W (2010) Transmutations of ancient settlements and environmental changes between 6000 and 2000 a BP in the Chaohu Lake Basin, East China. J Geogr Sci 20:687–700

Wu W (1983) Holocene palaeogeography of the Hangzhou Bay. Acta Geogr Sin 38:113–126 (in Chinese)

Xie SC et al (2013) Concordant monsoon-driven postglacial hydrological changes in peat and stalagmite records and their impacts on prehistoric cultures in central China. Geology 41:827–830

Xu QH, Xiao JL, Li YC, Tian F, Nakagawa T (2010) Pollen-based quantitative reconstruction of Holocene climate changes in the Daihai Lake area, Inner Mongolia, China. J Clim 23:2856–2868

Yancheva G et al (2007) Influence of the intertropical convergenze zone on the East Asian monsoon. Nature 445:74–77

Yang XD, Wang SM, Tong GB (1996) Character of palynology and changes of monsoon climate over the last 10000 years in Gucheng Lake, Jiangsu Province. Acta Bot Sin 38:576–581 (in Chinese)

Yang XL, Liu JB, Liang FY, Yuan DX, Yang Y, Lu YB, Chen FH (2014) Holocene stalagmite $\delta^{18}O$ records in the East Asian monsoon region and their correlation with those in the Indian monsoon region. Holocene 24:1657–1644

Yao P, Huang CC, Pang JL, Zha XC, Li XG (2008) Palaeoflood hydrological studies in the middle reaches of the Beiluohe River. Acta Geogr Sin 63:1198–1206 (in Chinese)

Yi S, Saito Y, Yang DY (2006) Palynological evidence for Holocene environmental change in the Changjiang (Yangtze River) delta, China. Palaeogeogr Palaeoclimatol Palaeoecol 241:103–117

Yi S, Saito Y, Zhao Q, Wang P (2003) Vegetation and climate changes in the Changjiang (Yangtze River) Delta, China, during the past 13,000 years inferred from pollen records. Quat Sci Rev

22:1501–1519

Yu XF, Zhou W, Franzen LG, Feng X, Peng C, Jull AJT (2006) High-resolution peat records for Holocene monsoon history in the eastern Tibetan plateau. Sci China Ser D Earth Sci 49:615–621

Zhang Q, Zhu C, Liu CL, Jiang T (2005) Environmental change and its impacts on human settlement in the Yangtze Delta, P.R. China. Catena 60:267–277

Zhao J, Chen CK (1999) Chinese Geography (in Chinese). Higher Education Press, Beijing

Zhao P, Zhu Y, Zhang R (2007) An Asian-Pacific teleconnection in summer tropospheric temperature and associated Asian climate variability. Clim Dyn 29:293–303

Zhao XH, Feng XS (2014) Periodicities of solar activity and the surface temperature variation of the Earth and their correlations. Chin Sci Bull 59:1284–1292

Zhao Y, Yu Z, Chen F, Zhang J, Yang B (2009) Vegetation response to Holocene climate change in monsoon-influenced region of China. Earth Sci Rev 97:242–256

Zheng Z et al (2008) Comparison of climatic threshold of geographical distribution between dominant plants and surface pollen in China. Sci China Ser D Earth Sci 51:1107–1120

Zheng Z et al (2014) East Asian pollen database: modern pollen distribution and its quantitative relationship with vegetation and climate. J Biogeogr 41:1819–1832

Zhou X, Zhao P, Liu G (2009) Asian-Pacific Oscillation index and variation of East Asian summer monsoon over the past millennium. Chin Sci Bull 54:3768–3771

Zhu C, Chen X, Zhang GS, Ma CM, Zhu Q, Li ZX, Xu WF (2008) Spore-pollen-climate factor transfer function and paleoenvironment reconstruction in Dajiuhu, Shennongjia, central China. Chin Sci Bull 53:42–49

Zong Y, Chen Z, Innes JB, Chen C, Wang Z, Wang H (2007) Fire and flood management of coastal swamp enabled first rice paddy cultivation in east China. Nature 449:459–462

Zong Y, Innes JB, Wang Z, Chen Z (2011) Mid-Holocene coastal hydrology and salinity changes in the east Taihu area of the lower Yangtze wetlands, China. Quat Res 76:69–82

Zong Y, Lloyd JM, Leng MJ, Yim WWS, Huang G (2006) Reconstruction of Holocene monsoon history from the Pearl River estuary, southern China, using diatoms and carbon isotope ratios. Holocene 16:251–263

Zong Y, Wang Z, Innes JB, Chen Z (2012) Holocene environmental change and Neolithic rice agriculture in the lower Yangtze region of China: a review. Holocene 22:623–635

## Figure captions

**Figure 1** Mean 700 hPa atmospheric airstream lines between June and August based on the NCEP/NCAR Reanalysis data during the time interval of 1971–2000 (Kalnay et al. 1996). Blue plus signs correspond to the localities of three fossil sites (Chaohu, Gucheng, and Pingwang) in the lower reaches of the Yangtze basin. ISM, EASM, and Westerlies indicate the regions dominated by the Indian and Eastern Asian summer monsoon, as well as westerly air circulation, respectively. Green dashed line shows the present-day northern boundary of the Asian summer monsoon system modified from Chen et al. (2008).

**Figure 2** Numerical performance of the calibration models for mean total annual precipitation (PANN) as well as mean annual temperature (TANN) based on pollen data. Statistical parameters consist of coefficient of determination ($R^2$) between observed and predicted values, root-mean-square-error of prediction (RMSEP), and maximum (Max.) bias.

**Figure 3** Pollen-based quantitative reconstructions for PANN with RMSEP of 232.06 mm and TANN with RMSEP of 3.62 °C at Chaohu, Gucheng and Pingwang over the last 10,000 years.

**Figure 4** Pollen-based PANN and TANN estimates during the last 10,000 years for the lower Yangtze region of China derived from the six reconstructions in Figure 3.

**Figure 5** Power spectrum analyses for the pollen-stacked PANN and TANN records spanning the past 10,000 years.

**Figure 6** Holocene comparison of pollen-estimated **a** PANN and **b** TANN sequences for the lower Yangtze region (LYR) of China with other related climatic records including: **c** mean summer solar insolation (SI) at 65 °N (Laskar et al. 2004); stalagmite $\delta^{18}O$ series from **d** Dongge (Dykoski et al. 2005), **e** Sanbao (Wang et al. 2008), and **f** Qunf (Fleitmann et al. 2003) Caves; **g** Kiel Climate Model (KCM)-based PANN simulation for southwestern China (Chen et al. 2014); pollen-derived **h** PANN reconstruction for Xingyun Lake in Yunan Province (Chen et al. 2014) and **i** TANN reconstruction for Dajiuhu wetland in Hubei Province (Zhu et al. 2008); pollen-composited **j** moisture index (MI; Zhao

et al. 2009) and **k** tree cover (TC; Tian et al. 2016) records for southern China (SC); **l** humification (H) record from Hongyuan wetland on the southeastern Tibetan Plateau (Yu et al. 2006); **m** moisture index (MI) synthesized from various proxy data from the southern Tibetan Plateau (ST; Ran and Feng 2013); records of **n** total organic carbon (TOC; Yancheva et al. 2007) and **o** tree pollen percentage (TP; Wang et al. 2007) from Huguangyan Maar Lake in SC; **p** Indian summer monsoon (ISM) index synthesized for monsoonal China (Wang et al. 2010); **q** Intertropical Convergence Zone (ITCZ) index from Venezuela (Haug et al. 2001); **r** *Globigerina bulloides* percentage record from ODP Site 723 in Arabian Sea (AS; Gupta et al. 2005); **s** and **t** composite sea surface temperature (SST-1 and SST-2) records for Western Pacific Warm Pool (WPWP; Scott et al. 2004; Koutavas and Joanides 2012); and **u** El Niño/Southern Oscillation (ENSO) index from Ecuador (Moy et al. 2002). The grey band depicts the moisture or thermal maximum during the early Holocene in southern China.

**Figure 7** Holocene comparison of pollen-inferred **a** PANN and **b** TANN records for the lower Yangtze region (LYR) of China with other climatic proxy records from northern China and other regions of the northern Hemisphere: pollen-reconstructed PANN records for **c** Gonghai Lake (Chen et al. 2015) on the Chinese Loess Plateau (CLP) and **d** Daihai Lake (Xu et al. 2010) in northern China (NC); **e** multi-proxy-based TANN sequence for NC (Hou and Fang 2011); **f** East Asian summer monsoon (EASM) index for monsoonal China (Wang et al. 2010); tree pollen records from **g** Qinghai Lake (Shen et al. 2005) and **h** Bayanchagan Lake (Jiang et al. 2006) in NC; **i** pollen-based moisture index (MI) for the EASM marginal region (Wang and Feng 2013); frequency distributions of palaeosol occurrences in **j** CLP (Wang et al. 2014) and **k** NC (Li et al. 2014); **l** frequency formations of loess or aeolian sands (AS) in NC (Li et al. 2014); **m** magnetic susceptibility (MS) record from the Yulin loess–palaeosol section on CLP (Lu et al. 2013); **n** moisture index (MI) synthesized for Arid Central Asia (ACA; Chen et al. 2008); melt water input (MI) from **o** the Laurentide Ice Sheet (Jennings et al. 2015) and **p** the Agassiz Ice Cap (Fisher et al. 2012); **q** ice-sheet coverage in northern Hemisphere (NH; Dyke 2004); and **r** Atlantic meridional overturning circulation (AMOC) index based on mean sortable silt grain size (SSGS) from core GS06-144 08GC in northern Atlantic Ocean (Mjell et al. 2015). The grey band shows the moisture or thermal maximum during the middle Holocene in northern monsoonal China. The pink band indicates the moisture or thermal maximum during the early Holocene in southern

692 monsoonal China.

693

694 **Table 1** Summary of fossil pollen datasets for PANN and TANN reconstructions at Chaohu, Gucheng

695 and Pingwang in the lower Yangtze region of China

696

| Site | Lat. (°) | Long. (°) | Elev. (m) | Num. dates | Res. (years) | Reference |
|---|---|---|---|---|---|---|
| Chaohu | 117.39 | 31.56 | 10 | 10 | 158 | Chen et al. (2009) |
| Gucheng | 118.9 | 31.28 | 6 | 4 | 30 | Yang et al. (1996) |
| Pingwang | 120.64 | 30.96 | 1.6 | 5 | 135 | Innes et al. (2014) |

697 Lat. = latitude; Long. = Longitude; Elev. = Elevation; Num. = Number; Res. (yrs) = Resolution
698 (years/sample)

699

700

701

702

703

704 **Figure 1**

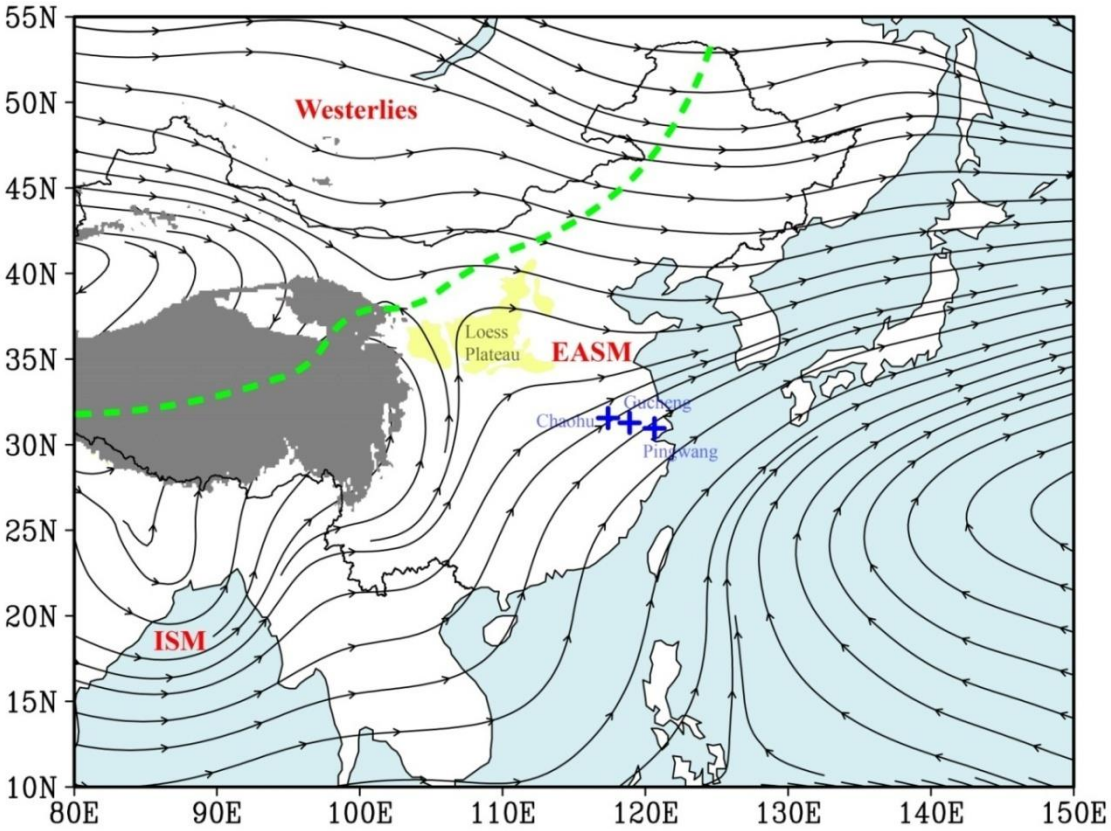
55N
50N
45N
40N
35N
30N
25N
20N
15N
10N
80E
90E
100E
110E
120E
130E
140E
150E
Westerlies
Loess
Plateau
EASM
Gucheng
Chaohu
Pingwang
ISM

**Figure 2**

721

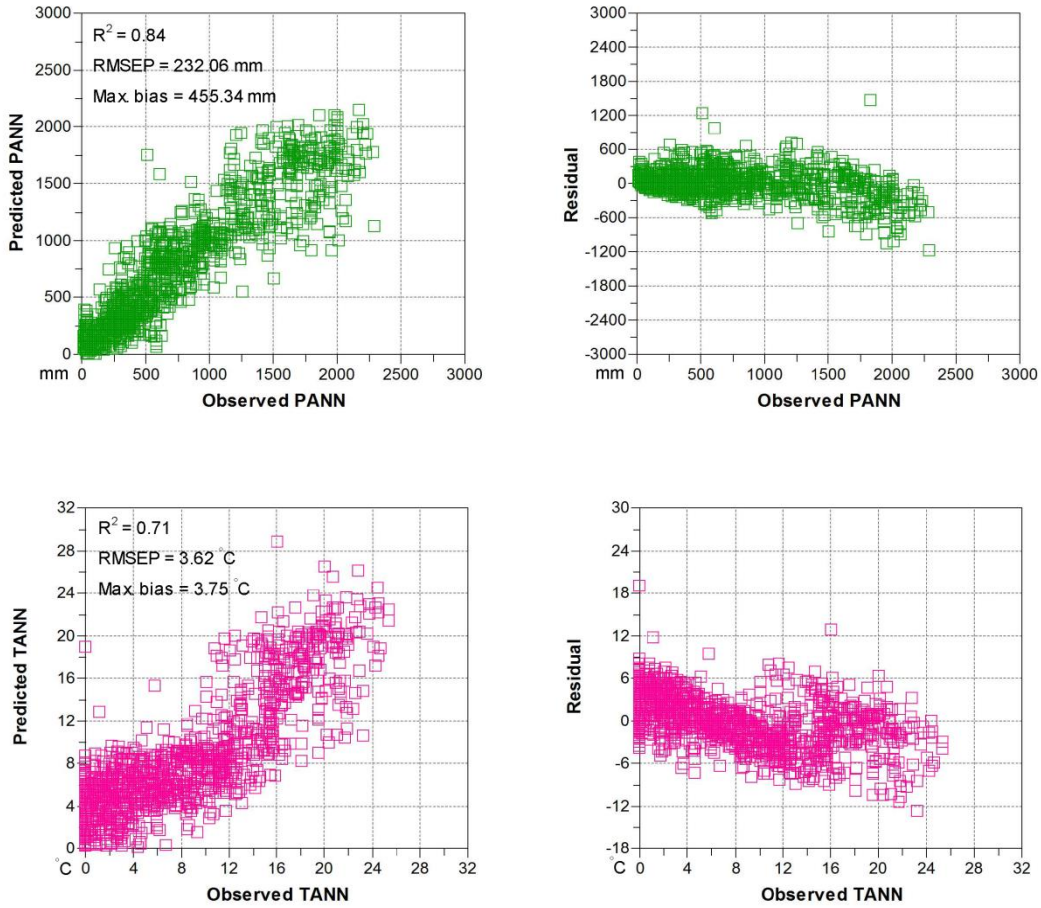


722

723 **Figure 3**

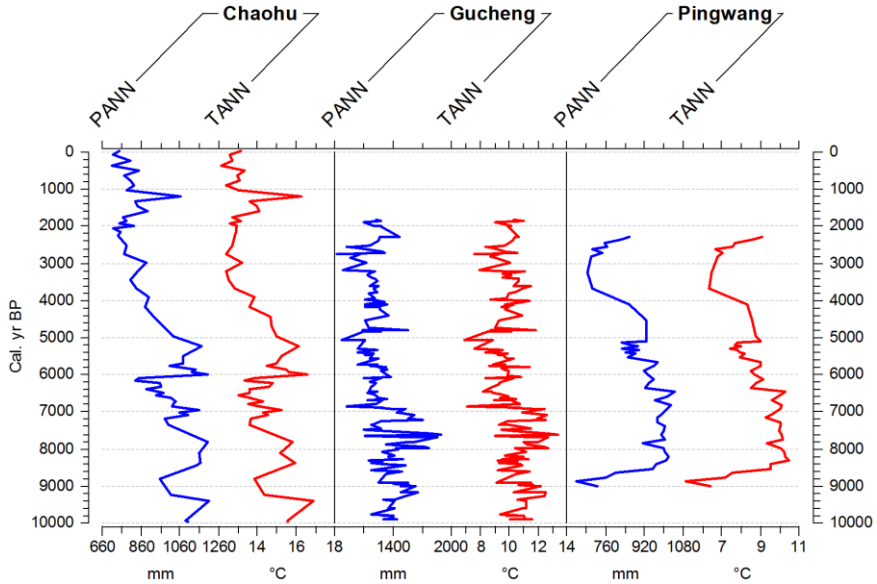


724

725

726 **Figure 4**

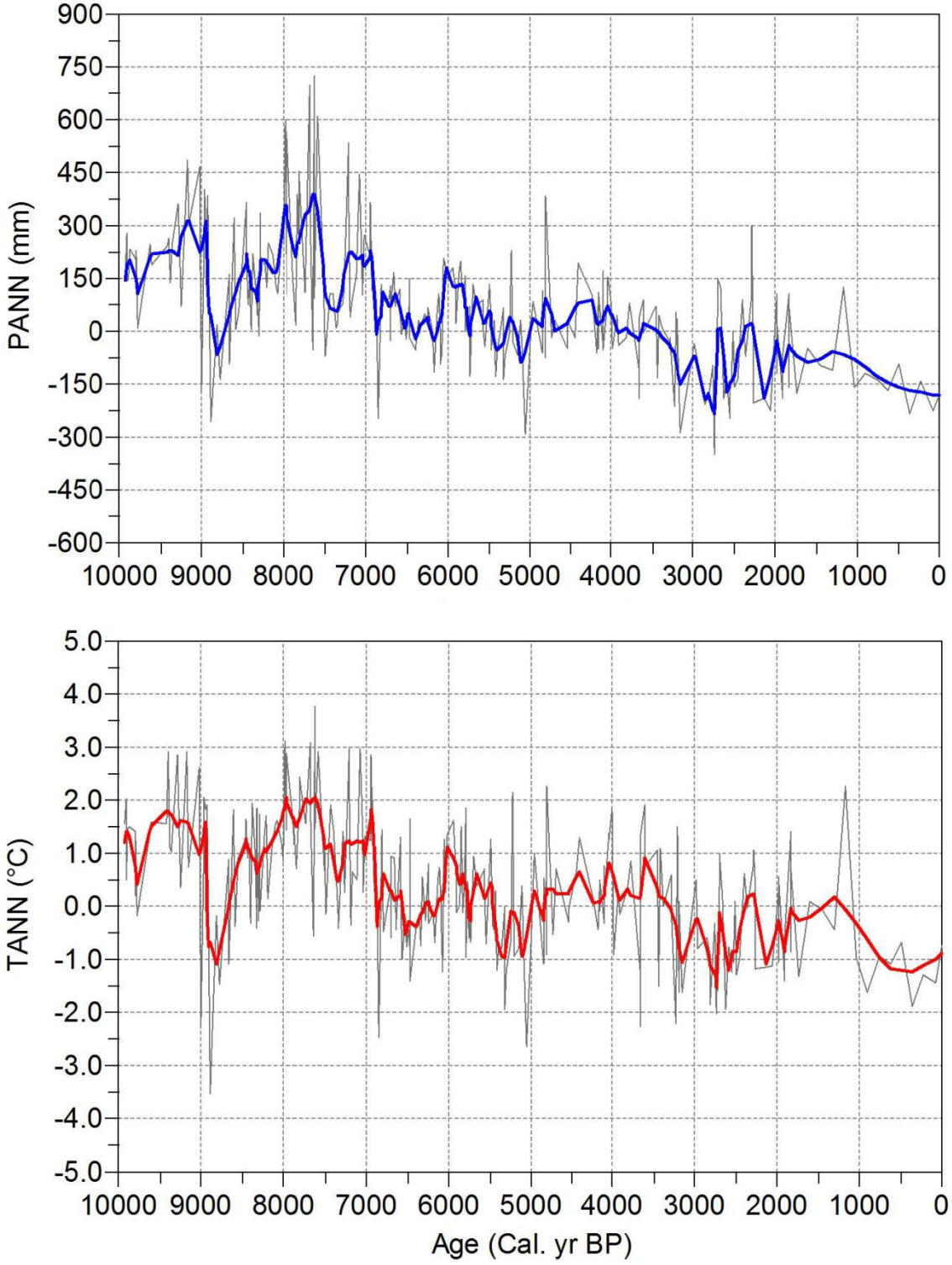


727

728

729

730 **Figure 5**

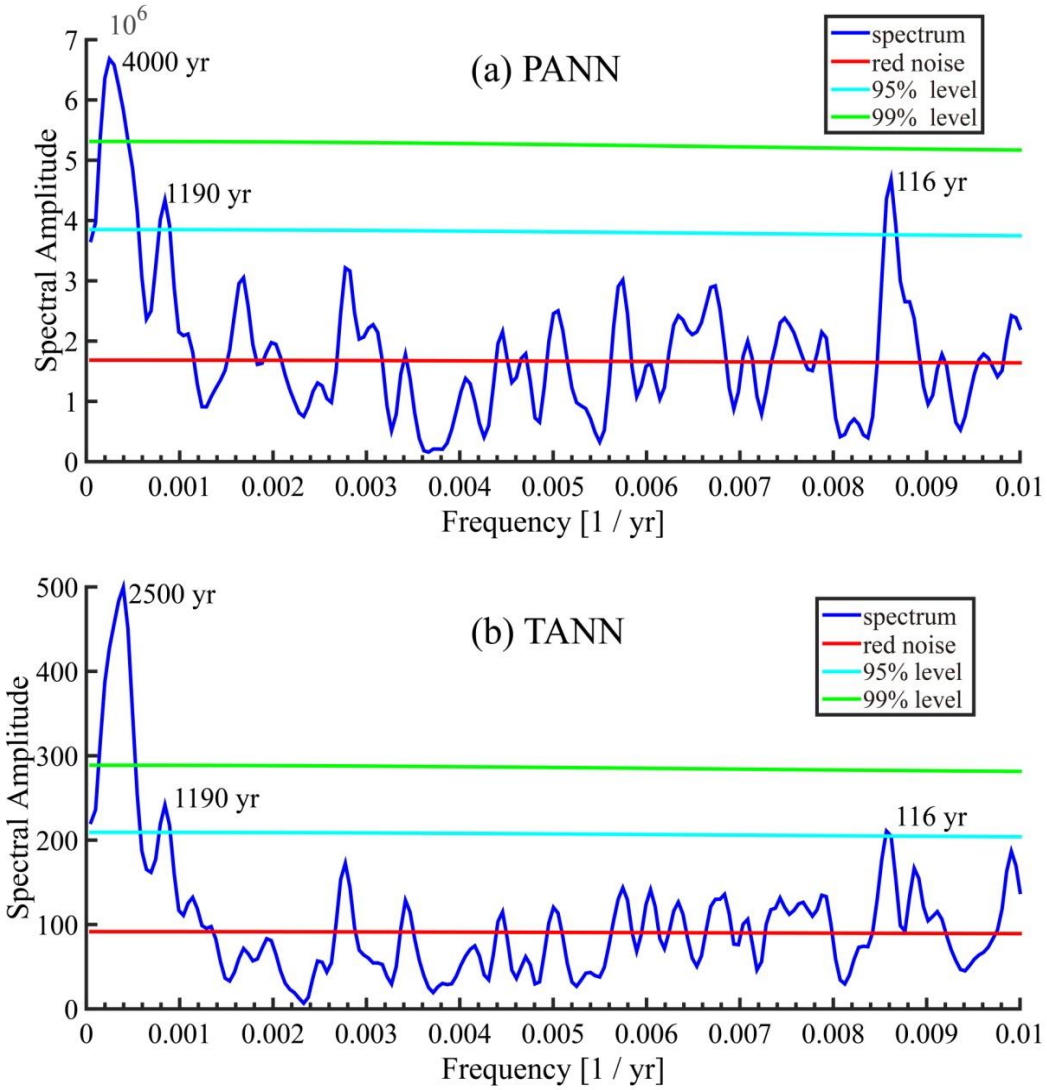
(a) PANN
$10^6$
4000 yr
1190 yr
116 yr
spectrum
red noise
95% level
99% level
Spectral Amplitude
Frequency [1 / yr]
(b) TANN
2500 yr
1190 yr
116 yr
spectrum
red noise
95% level
99% level
Spectral Amplitude
Frequency [1 / yr]

**Figure 6**

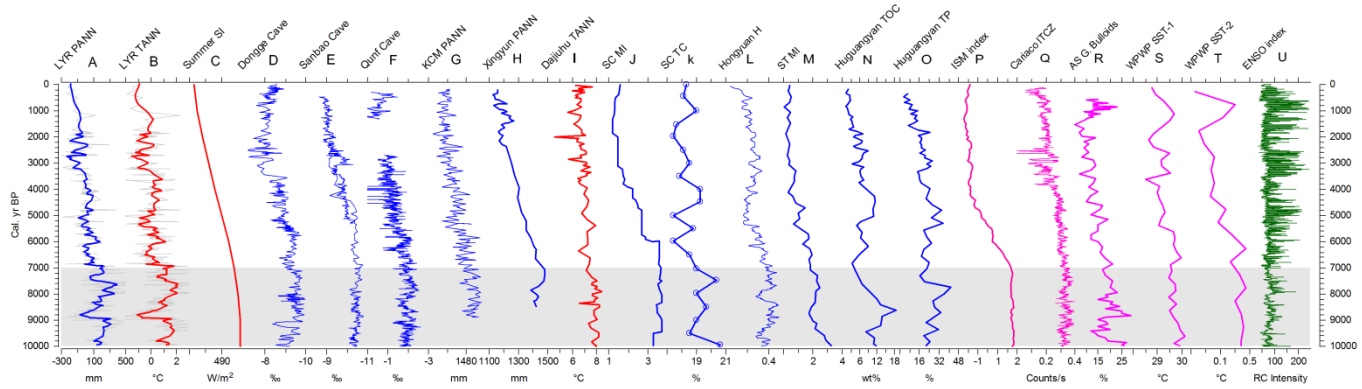
LYR PANN
LYR TANN
Summer SI
Dongge Cave
Sanbao Cave
Qunf Cave
KCM PANN
Xingyun PANN
Dajiuhu TANN
SC MI
SC TC
Hongyuan H
ST MI
Huguangyan TOC
Huguangyan TP
ISM index
Cariaco ITCZ
AS G. Bulloids
WPWP SST-1
WPWP SST-2
ENSO index
Cal. yr BP
mm
°C
W/m²
‰
‰
‰
mm
mm
°C
%
wt%
%
Counts/s
%
°C
°C
RC Intensity

**Figure 7**

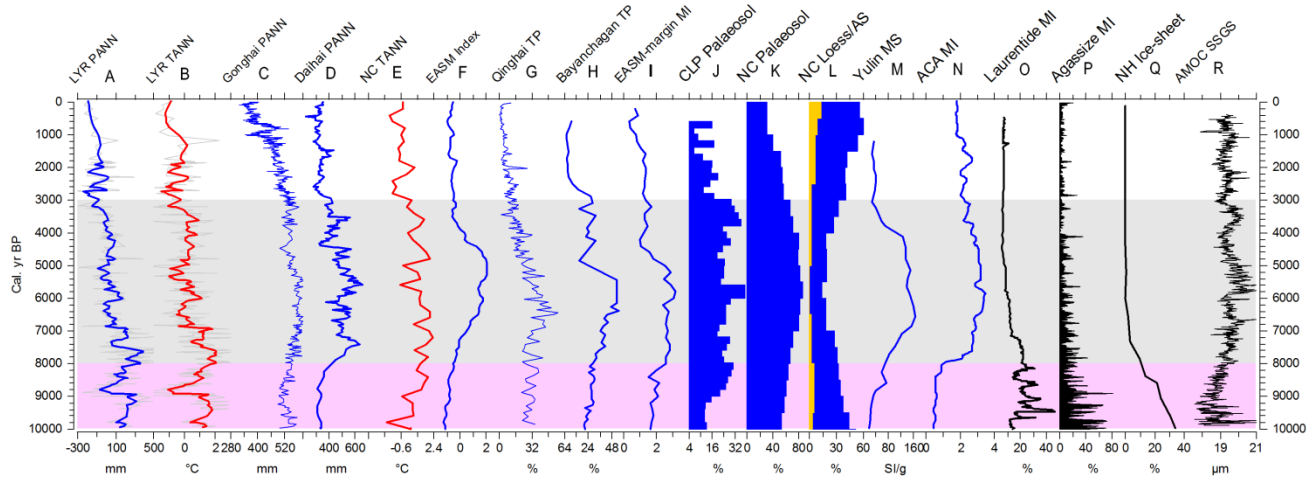
LYR PANN
LYR TANN
Gonghai PANN
Daihai PANN
NC TANN
EASM Index
Qinghai TP
Bayanchagan TP
EASM-margin MI
CLP Palaeosol
NC Palaeosol
NC Loess/AS
Yulin MS
ACA MI
Laurentide MI
Agassize MI
NH Ice-sheet
AMOC SSGS
Cal. yr BP
mm
°C
mm
mm
°C
%
%
%
%
%
SI/g
%
%
%
µm